

The Cool-Season Tornadoes of California and Southern Australia

BARRY N. HANSTRUM

Bureau of Meteorology, Perth, Western Australia, Australia

GRAHAM A. MILLS

Bureau of Meteorology Research Centre, Melbourne, Victoria, Australia

ANDREW WATSON

Bureau of Meteorology, Adelaide, South Australia, Australia

JOHN P. MONTEVERDI

San Francisco State University, San Francisco, California

CHARLES A. DOSWELL III*

NOAA/National Severe Storms Laboratory, Norman, Oklahoma

(Manuscript received 12 March 2001, in final form 13 February 2002)

ABSTRACT

Examples of cool-season tornadic thunderstorms in California and southern Australia are examined. Almost one-half of the reported Australian tornadoes and the majority of those in California occur in the cool season. It is shown that in both areas the typical synoptic pattern shows an active midlatitude trough just upstream, with a strong jet streak aloft. In both areas the tornadic thunderstorms occur with weak to moderate levels of thermodynamic instability in the lower troposphere but with extremely high values of low-level positive and bulk shear. Statistical tests on null cases (nontornadic thunderstorms) in the Central Valley of California indicate that large values of 0–1-km shear provide a discriminator for more damaging (F1–F3) tornadoes, whereas bulk measures of buoyancy, such as CAPE, do not. Australian case studies and tornado proximity soundings show similar characteristics. A “cool-season tornadic thunderstorm potential” diagnostic for Australian conditions, based on regional NWP analyses and forecasts, is described. It identifies those locations at which negative 700-hPa surface lifted index, near-surface convergence, and surface–850 hPa shear $>11 \text{ m s}^{-1}$ are forecast to occur simultaneously, and it shows considerable potential as an objective alert for forecasters. During the winter of 1996, all nine occasions on which tornadoes were reported were successfully identified in 24-h forecasts. After a variety of assessments suggested the value of this diagnostic, and following positive forecaster feedback during preoperational trials, it became an operational forecast product in May of 2000.

1. Introduction

Damaging tornadic thunderstorms are widely associated with the high-buoyancy, high-shear environments common over the Great Plains in the spring and early summer, as described in, for example, Davies-Jones (1986). However, tornadic thunderstorms are also well

known to occur in other less- (but still positively) buoyant environments. These include the Great Plains cool-season environment (Johns et al. 1993, hereinafter JDL), the landfalling tropical cyclone environment (McCaul and Weisman 1996), the California environment (Blier and Batten 1994; Monteverdi and Quadros 1994), and the cool-season environment in southern Australia (Foley and Hanstrum 1990; Hanstrum et al. 1998).

California tornadic storms occur in preferred locations—the Central Valley, the south coast, the north-central coast, and the southeast deserts (Blier and Batten 1994). In the first three zones, these storms occur preferentially during the cool season, with over 90% of Central Valley tornadic storms occurring in that period. Most of these tornadoes are at the weaker end of the F-

* Current affiliation: Cooperative Institute for Mesoscale Meteorological Studies, Norman, Oklahoma.

Corresponding author address: Graham A. Mills, Bureau of Meteorology Research Centre, Box 1289K Melbourne, VIC 3001, Australia.
E-mail: g.mills@bom.gov.au

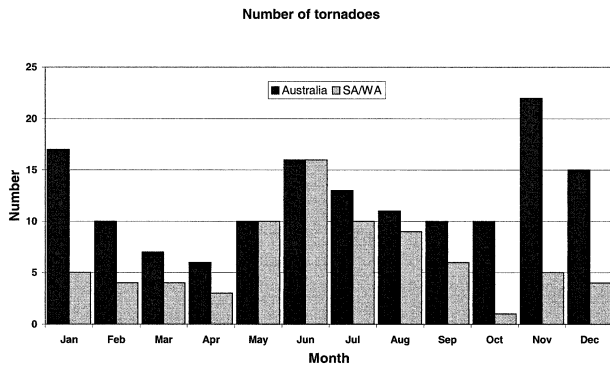


FIG. 1. Total number of tornadoes in Australia (black) and for the states of South Australia and Western Australia combined (gray) for each month for the 10 yr, 1987–96.

scale range, but the coincidence of their areas of occurrence and areas of significant population density makes it important to forecast these events.

More than 700 tornadoes have been recorded in Australia since European settlement more than 200 years ago. Over 40 lives have been lost. Since many thunderstorms occur over the sparsely populated inland regions of the country, and the official documentation of events in the early part of the record is sketchy and incomplete, the actual number of tornadoes is undoubtedly much higher. Storm-spotter networks, first established in Australia during the mid-1980s, now include more than 5000 volunteers who report severe storm events to the Australian Bureau of Meteorology's (BoM) regional offices. This has led to an increase in the number of reported tornadoes: in the decade from 1987 to 1996, there were 162 tornadoes reported—more than one-quarter of the total number previously recorded. The monthly frequency of all Australian tornado reports from 1987 to 1996 inclusive (Fig. 1) shows a bimodal distribution, with peaks in midwinter and early summer. Almost one-half of the tornadoes occur during the months from May to September (late autumn to early spring in the Southern Hemisphere). Further, Fig. 1 shows that the vast majority of these cool-season tornadoes occur in South Australia (SA) and Western Australia (WA). This geographic bias is demonstrated in Fig. 2, which shows that for this 10-yr period, these cool-season tornadoes overwhelmingly occurred in two preferred areas: the southwest of WA and the southeast coastal areas of SA (the number of events is less than the number of tornado reports in Fig. 1 because some events resulted in more than one tornado report). They can occur at any time of the day but are more frequent during mid- to late afternoon. Although they tend to have strengths at the lower end of the F scale, there have been strong, long-lived cool-season tornadoes in Australia (Clarke 1962; Brook 1965; Phillips 1965; Watson 1985, 1996; Hanstrum 1994). Because the preferred areas of occurrence of these storms coincide with the most densely populated areas of WA and SA, and in-

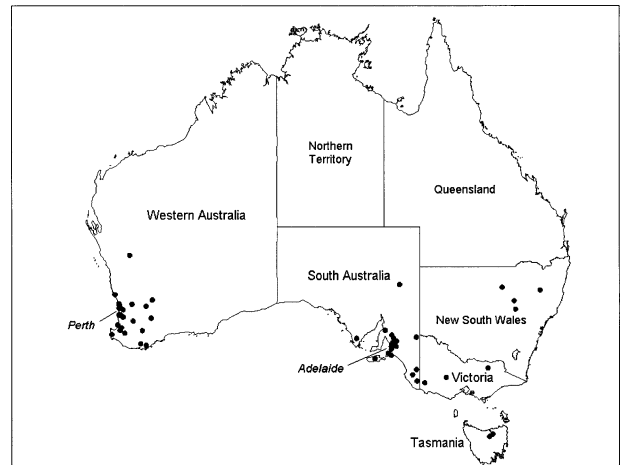


FIG. 2. Map showing the locations of cool-season (May–Sep) tornado reports in the period 1987–96.

clude the capital cities of these two states, Perth and Adelaide, there is a significant community need for accurate warnings of these events.

The goal of this research has been to increase the understanding of the environments in which these cool-season tornadoes occur. Although the work on the California and Australia tornadoes began independently, it became clear that the events in these different geographic locations had some common traits. Hence, it was decided to work together to develop methods for identifying from numerical weather prediction (NWP) model guidance the environments in which these storms may occur. This work has four main components. First, two Australian case studies will be presented, to document the typical synoptic environment in which these storms form, and to compare this with the typical California environment summarized in Fig. 1 of Lipari and Monteverdi (2000, hereinafter LM). Using analyses of proximity soundings from both California and Australia, it will be shown that these storms occur in similar relatively low buoyancy, but high low-level positive shear, environments and that this shear–buoyancy space has the potential to discriminate these tornadic environments. Third, applying these concepts to numerical analyses and predictions in Australia, it is shown that there is indeed considerable potential to predict these environments in 24-h NWP forecasts.

Last, it is shown that while the California and Australian synoptic environments are broadly similar, the individual topographic features do make their details different. These environments are compared with other low-buoyancy/high-shear environments in which tornadoes have been reported, including that of landfalling tropical cyclones (McCaul and Weisman 1996). These similarities, another Australian low-buoyancy tornadic thunderstorm environment identified in this study, and some implications of this work will be discussed.

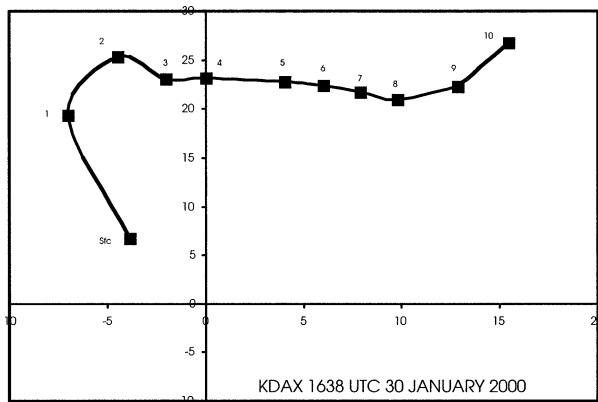


FIG. 3. Hodograph of KDAX VAD for 1638 UTC 30 Jan 2000. Wind components: m s^{-1} . Elevations: 10^3 ft.

2. Synoptic environment of cool-season tornadoes

a. California storms

California tornadic thunderstorms are generally low topped with equilibrium levels between ~ 8 and 11.5 km and occur under the relatively low tropopause heights of the winter and spring months (Carbone 1983; Monteverdi and Quadros 1994). Some of these have been shown to have supercellular characteristics (Monteverdi and Quadros 1994; Monteverdi and Johnson 1996). Lipari and Monteverdi (2000) present a schematic of the synoptic environment associated with tornadic thunderstorms in California's Central Valley. A very favorable shear environment is created there as a surface front and associated short-wave trough-jet streak crosses the California coast. With the front typically south of the Central Valley, topographic channeling east of the leeside trough acts to create surface southeasterly flow east of the air mass that is subsiding from the Coast Range. These southeasterly winds can contribute to warm advection (and ascent) to the north of the synoptic-scale cold front. Other areas can also experience locally backed flow and finally, at least in the Sacramento River valley, a barrier jet can form about 1500 ft AGL, as seen in the example in Fig. 3. All these factors contribute to extremely large values of low-level bulk¹ and positive² shear, as evidenced by strongly anticyclonically curved hodographs.

Rotunno and Klemp (1982), McCaul (1993), and Wicker and Cantrell (1996), among others, have shown that dynamically induced perturbation pressure forces associated with an anticyclonically turning wind shear vector within a layer having significant buoyancy can augment the updraft by a factor of 2 to 3. This updraft

augmentation may help to explain some reported occurrences of hail ≥ 2 cm produced by low-topped storms in a low-buoyancy environment, if that environment is sufficiently cold. With the positive shear in these California storm environments being concentrated in the lower levels, the resulting nonbuoyant pressure perturbation forces generally act in the same layer (below 500 hPa) where most of the buoyancy is found.

b. Australian storms—Southwest Australia 7 June 1995

Three F2 tornadoes occurred over southwest WA during the midafternoon (between 0600 and 0800 UTC³) on 7 June 1995. Two of these, T1 and T2 in Fig. 4, occurred in the convergent low-level flow ahead of a cold front associated with an intense midlatitude depression, while the third, T3, occurred along a prefrontal trough. Tornado T1 had the longest path length (>70 km) with a path width that varied between 50 and 100 m. The Perth airport upper winds at 0500 UTC 7 June 1995 were modified using the hourly surface winds from an Automatic Weather Station (AWS) 50 km from where the track of T1 commenced. Winds turned anticyclonically with height in the lowest kilometer, with a rapid increase in wind speed from 6 m s^{-1} at the surface to 20 m s^{-1} at 1 km. The magnitude of the surface-to-1-km shear was 16 m s^{-1} . (Note that in this case study, and in the next, there are some unavoidable uncertainties in the magnitudes of shear and instability due to the separation in time and space between event locations and the nearest rawinsonde observations.)

Although the tornadic thunderstorm was outside the range of the Perth city radar, the movement of the cell was estimated from hourly IR satellite imagery to be from 290° at 25 m s^{-1} . The 0–3-km storm-relative helicity (SRH) calculated from the modified wind profile and using this estimated cell motion was -130 J kg^{-1} . The straight-line hodograph (Fig. 5) indicated that a small deviation to the left of the estimated storm motion would have resulted in a considerable increase in SRH. When modified to reflect the surface temperature conditions in the area at the time (temperature, 15°C ; dewpoint, 12°C), the Perth sounding at 2300 UTC 6 June 1995 gave a CAPE value of 345 J kg^{-1} (Fig. 6). The 700-hPa surface lifted index (SLI)⁴ was -2.5°C and the 500-hPa SLI was -2.1°C . Following the passage of the front, two weaker (F0) tornadoes occurred at Perth during the evening of 8 June 1995 as the axis of the cold air field crossed the WA coast. In contrast to the prefrontal tornado environment, the wind profile in the colder air turned cyclonically with height, from south-

¹ "Bulk shear" is the magnitude of the vector difference between the winds at the top and bottom of the layer.

² "Positive shear" is defined as the sum of the wind shear for the segments of the hodograph for which the wind turns anticyclonically or is unidirectional with height (Johns et al. 1993). Anticyclonic turning of the hodograph favors development of cyclonic supercells.

³ Western standard time is UTC plus 8 h.

⁴ The surface lifted index (SLI) is the difference between the 500-hPa temperature and the temperature of a surface parcel (with a known temperature and dewpoint) that is lifted dry-adiabatically to saturation, and then saturated adiabatically to 500 hPa.

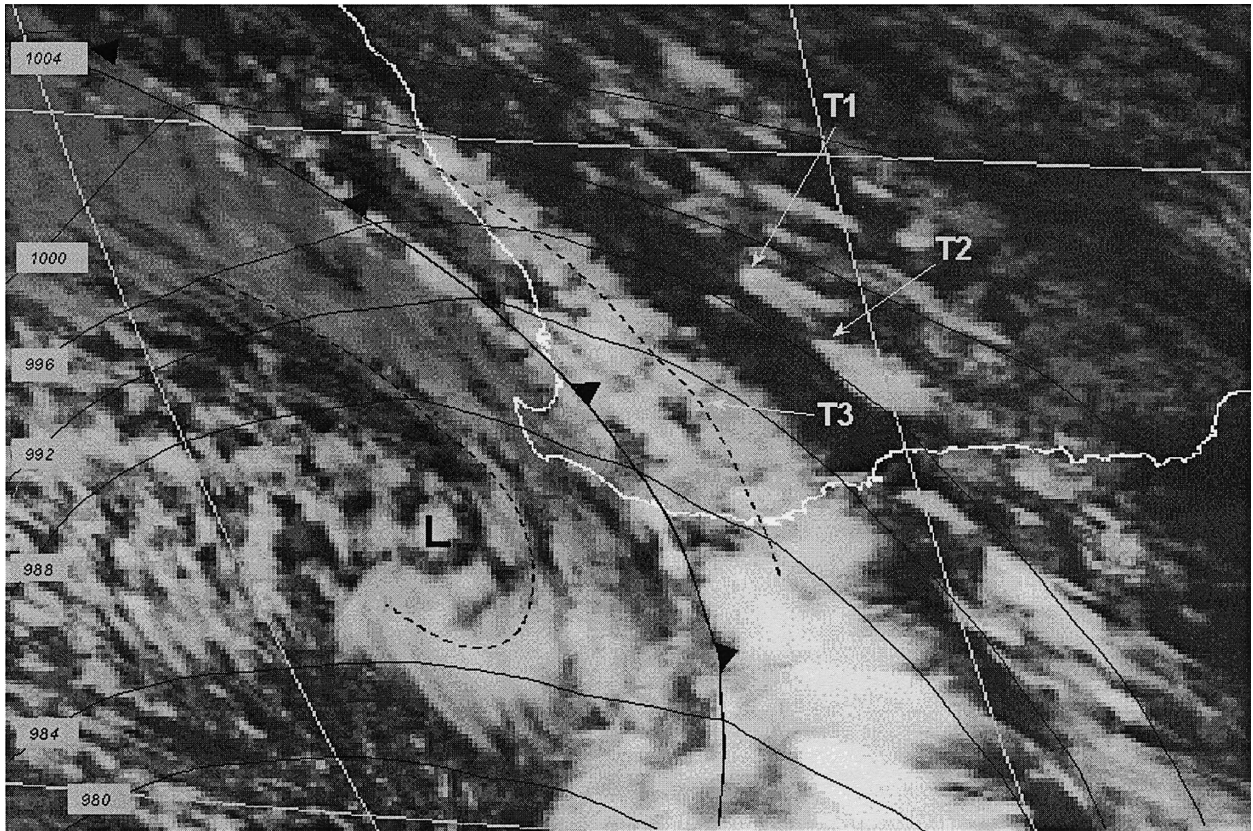


FIG. 4. Geostationary Meteorological Satellite-5 (GMS-5) IR satellite imagery for 0700 UTC [1500 local time (LT)] 7 Jun 1995 together with the MSLP analysis; contour interval is 4 hPa.

erly near the surface to westerly at 700 hPa. There was strong low-level shear, significant SRH (240 J kg^{-1}), and a CAPE of 500 J kg^{-1} .

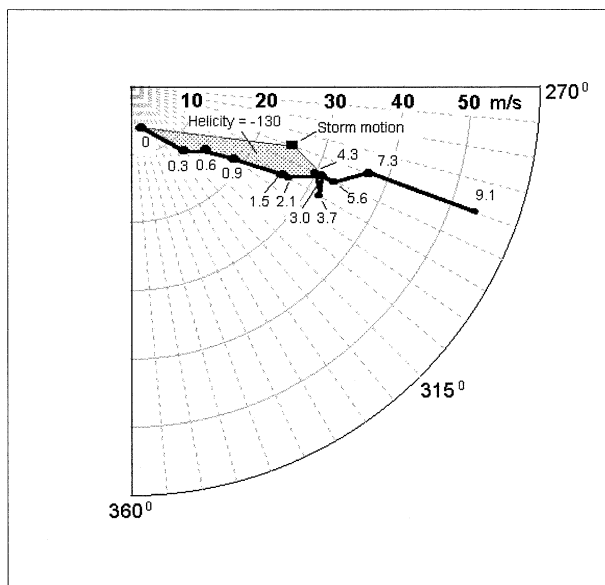


FIG. 5. Perth airport hodograph at 0500 UTC 7 Jun 1995. The surface wind has been modified to reflect conditions in the vicinity of T1. Levels: km; speeds: m s^{-1} .

c. Australian storms—South Australia 21 June 1995

Three F2 tornadoes were observed in southern SA between 0700 and 0800 UTC⁵ 21 July 1995. Damage surveys indicated pathlengths on the order of tens of kilometers, with one of the tornadic cells identifiable for almost 100 km. Path widths were on the order of 100 m. A strong midlatitude depression well south of SA was the dominant synoptic system (Fig. 7) in the region. A secondary low pressure center closer to the coast was associated with a surface cold front that extended northward through central SA. This front was moving east at about 15 m s^{-1} . The convective cells that produced two of the tornadoes can be seen (Fig. 8) in the visible satellite image at 0600 UTC 21 July 1995.

The tornadoes that caused damage in the Snowtown and Tarlee (Fig. 8) areas developed in an environment where surface temperatures were around 13°C and dew-points were between 8° and 10°C . Ascent along the sur-

⁵ Central standard time is UTC plus 9.5 h.

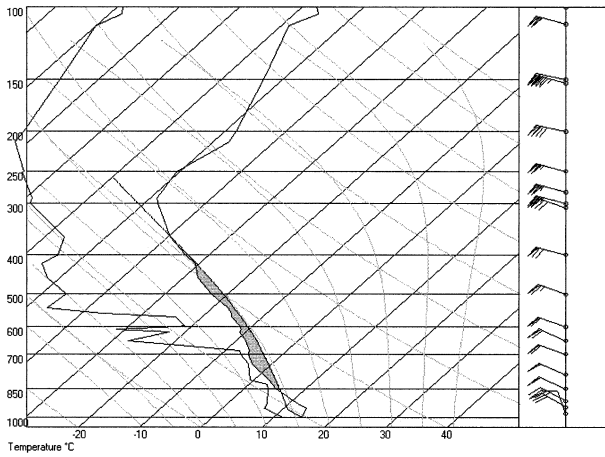


FIG. 6. Perth airport temperature sounding at 2300 UTC 6 Jun 1995 and wind profile at 0500 UTC 7 Jun 1995.

face cold front appeared to play a major role in initiating convection. Surface heating during the afternoon, albeit weak, contributed to destabilization of the lower atmosphere. The Adelaide Airport sounding at 1100 UTC, modified using the surface temperatures near the time of the events (Fig. 9), gave a CAPE value of 385 J kg^{-1} .

The wind profile in the lowest kilometer showed anti-cyclonic turning and an increase in wind speed from 10 m s^{-1} at the surface to 21 m s^{-1} at 1500 m above the surface (Fig. 10). The magnitude of the surface to 1-km positive shear was 12 m s^{-1} . Using radar-based estimates of storm movement from 295° at 26 m s^{-1} and the 0530 UTC vertical wind profile from the Adelaide airport, the environmental 0–3-km SRH was around -200 J kg^{-1} for these two storms.

There was no clear signature of a surface wind discontinuity for the third tornado that produced damage near Cummins. The movement of this storm, estimated from satellite imagery, was from 275° at 26 m s^{-1} . Storm-relative helicity (based on the 1130 UTC vertical wind profile from the Adelaide airport) was around -250 J kg^{-1} .

3. Shear and buoyancy values

a. California storms

Using 30 cases of tornadic thunderstorms in northern and central California during the period 1990–94, LM showed that these situations were characterized by large values of positive low-level shear. To document these

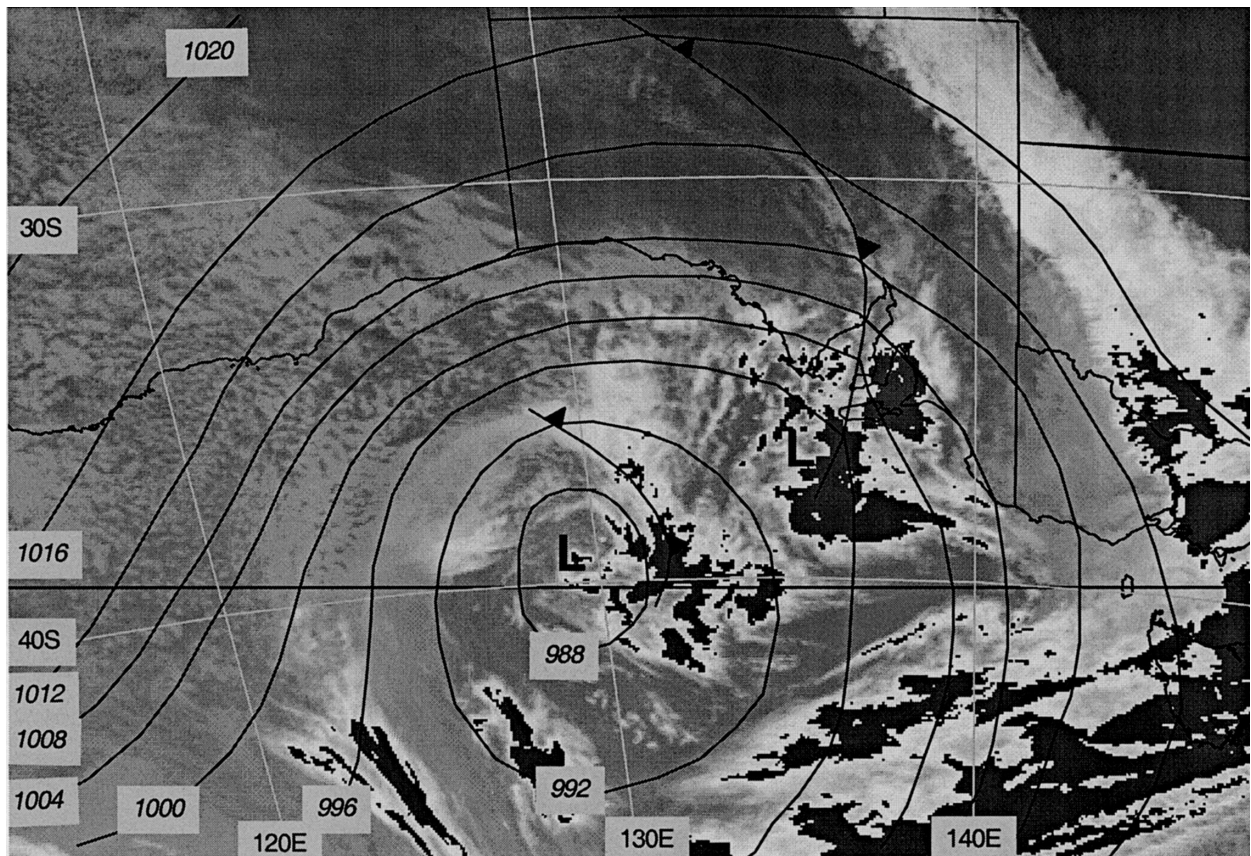


FIG. 7. GMS-5 enhanced IR satellite imagery for 0700 UTC (1630 LT) 21 Jul 1995, together with the MSLP analysis. Contour interval is 4 hPa.

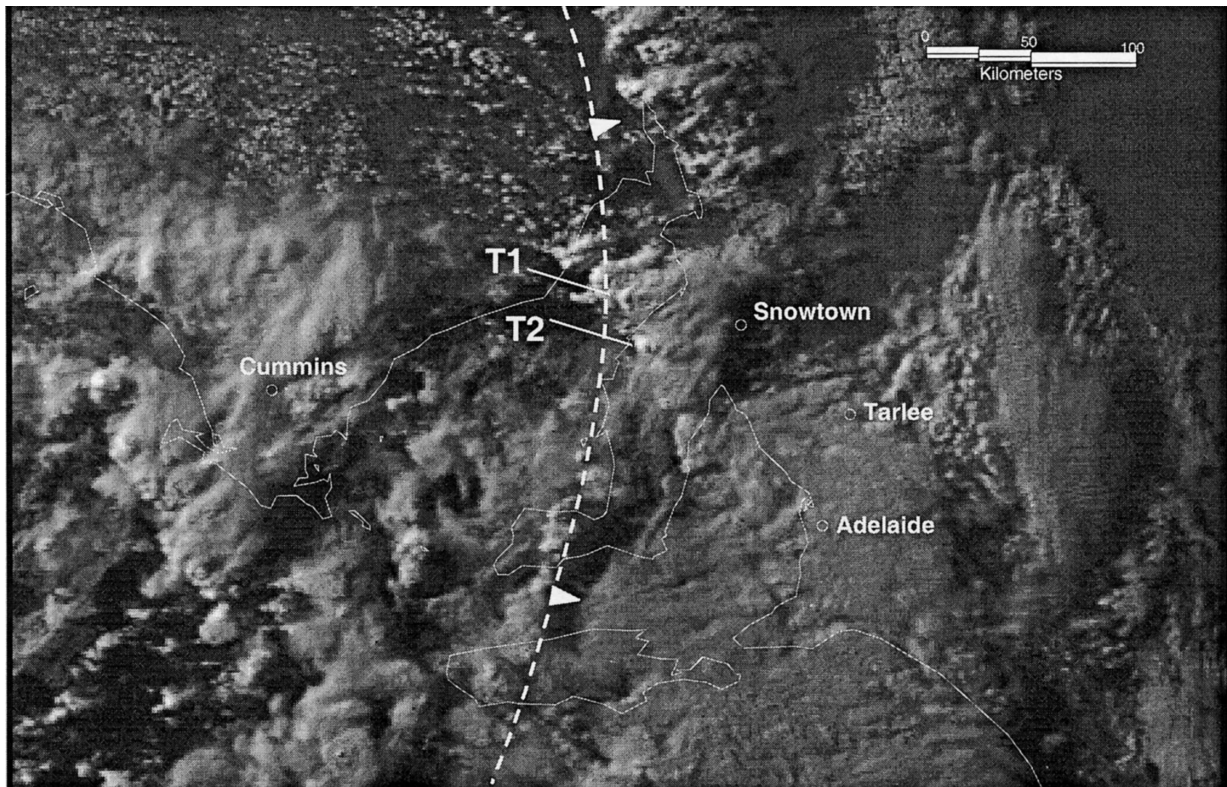


FIG. 8. GMS-5 visible satellite image at 0600 UTC 21 Jul 1995. Locations of towns, two of the tornadic cells (T1 and T2), and the surface cold front are marked.

relationships more systematically, LM's dataset has been augmented with a study of 40 "null" cases, defined as all days in the period 1990–94 for which *thunderstorms* were observed either at Sacramento, California (KSAC), or Fresno, California (KFAT), but *no tornadoes* were recorded in *Storm Data*. This is specifically intended to determine whether there are identifiable differences in buoyancy and/or shear between tornadic and

nontornadic thunderstorm environments in the Central Valley.

Buoyancy for each of the thunderstorm cases was obtained from the SHARP (Hart and Korotky 1991) output of surface-based CAPE (SCAPE), as were the values summarized in LM. In all cases, the Oakland, California (KOAK), rawinsonde data were modified by the surface temperature, dewpoint, and wind information at either KSAC or KFAT for the hour closest in time to thunderstorm occurrence. Both positive and bulk shears were calculated for the layers 0–1, 0–2, 0–3, and 0–6 km, all above ground level. The calculation of bulk shear is unambiguous, but the calculation of positive shear values can be sensitive to small curvature changes in the hodograph. However, the strongly curved hodographs present in California tornadic patterns generally make the positive shear values meaningful.

More than one-half of the 70 events considered in the sample occurred in the cool season (November–April). Interestingly, 28 of 30 tornado events were in the cool season; 21 of 40 null events occurred in the warm season. These proportions reflect the overall climatology of events in northern and central California: that is, most California tornadoes occur in the cool season, whereas thunderstorms in California are as likely to occur during the early and/or late warm season (i.e., in June or September) as they are during the cool season months. Al-

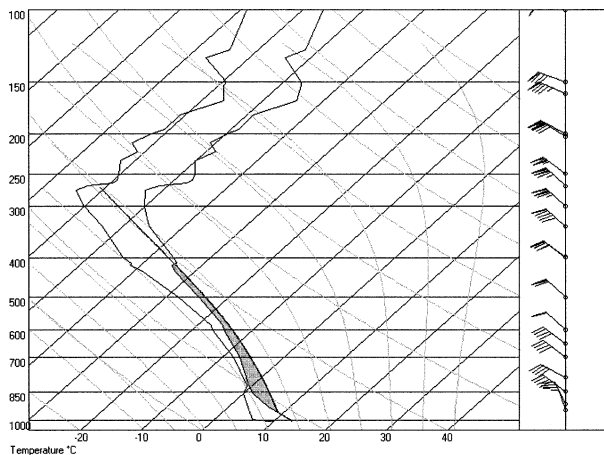


FIG. 9. Adelaide airport temperature sounding at 1100 UTC 21 Jul 1995 and wind profile at 0500 UTC 21 Jul 1995.

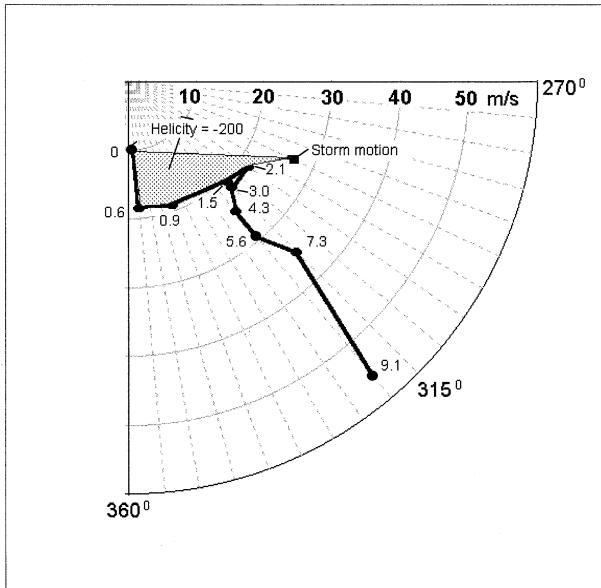


FIG. 10. Adelaide airport hodograph at 0500 UTC 21 Jul 1995, modified to reflect surface winds near where the Snowtown and Tarlee tornadoes formed. Levels: km; speeds: m s^{-1} .

though the null events and tornado events are not distributed through the year in the same way, this does not necessarily diminish the value of a comparison between their environments.

For all California tornadoes, the median CAPE is less than 500 J kg^{-1} (Fig. 11). A Student's t test performed by pairing CAPE for null, F0, and F1–F2 tornadic classes failed to show statistically significant difference at the 90% level between the CAPE values for each of these classes. That is, in this dataset, there is no statistical evidence for a relationship between bulk measures of buoyancy and the potential for thunderstorms to be associated with tornadoes. It is interesting to note that the largest values of the mean and maximum buoyancy occurred in the null category. These results are inconsistent with the notion that the greater the buoyancy, the greater the risk for tornadic convection (although obviously some buoyancy is a necessary ingredient for convection).

However, box and whiskers plots of the positive shear values emphasize the striking differences between the shear values for the F1–F2 cases and those for either the null or the F0 cases (Fig. 12). While the differences between the shear values for any of the layers in the F0 bin and the shear values for the same layers in the null bin are not statistically significant, the differences between the 0–1 and 0–2-km shear values in the F1–F2 bin and those in the other bins are statistically significant at the 95% level. Bulk shear distributions (not shown) are similar. This supports the hypothesis that a controlling factor in whether thunderstorms become tornadic is the strength of the low-level shear in the buoyant inflow layer, and that more intense storms in these

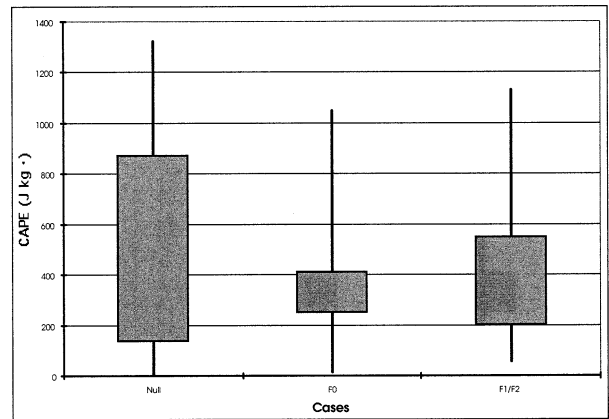


FIG. 11. Maximum, 75th, and 25th percentile and minimum values of SCAPE observed for the null, F0, and F1–F2 bins for northern and central California tornado cases, 1990–94.

low buoyancy environments are associated with stronger 0–1- and 0–2-km positive shear. Indeed, the shear values observed with the F1–F2 events were consistent with those observed with supercell thunderstorms observed elsewhere in the country (Johns and Doswell 1992). Although radar data for these events are not available and, therefore, the presence or absence of radar-detectable mesocyclones cannot be demonstrated, Fig. 12, in combination with Fig. 11, provides indirect evidence that suggests that most, if not all, of the F1–F2 events were supercellular, while at least some of the F0 events were nonsupercellular events.

b. Shear and buoyancy characteristics of Australian events

Tornado events that occurred in SA and WA during the Southern Hemisphere cool season, May–September, were extracted from the Australian Severe Thunderstorm Database for the period 1987–96. If more than

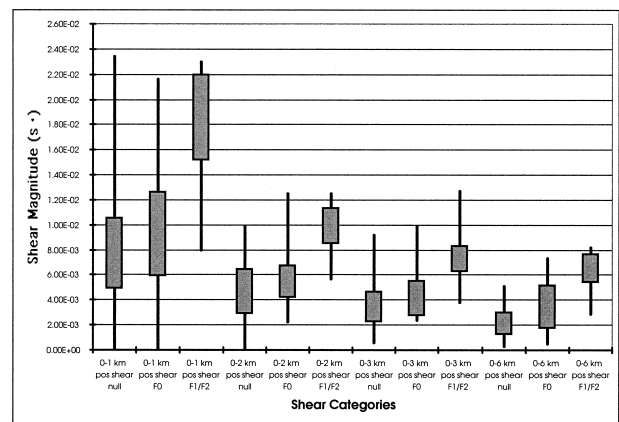


FIG. 12. Maximum, 75th, and 25th percentile and minimum values of positive shear observed for the null, F0, and F1–F2 bins for northern and central California tornado cases, 1990–94.

TABLE 1. Summary of parameter values for tornado environments in southwest WA and southern SA. Positive shear values are 10^{-3} s^{-1} . SLI is surface lifted index ($^{\circ}\text{C}$).

	No.	CAPE (J kg^{-1})	700-hPa SLI	500-hPa SLI	Positive shear 0–1 km	Positive shear 0–2 km	Positive shear 0–3 km	Positive shear 0–6 km
WA (F0)	7	240	-0.3	1.2	16.4	10.6	7.9	4.9
WA (F1–F3)	8	380	-1.0	-0.2	20.6	13.1	9.3	7.0
SA (all)	14	290	-1.4	0.4	14.9	10.4	7.7	4.4
All events	29	303	-1.0	0.4	16.8	11.2	8.2	5.9

one tornado was reported during a given event, then surface conditions for the location closest to the rawinsonde were used, and there were missing data for a few events. This left 32 proximity soundings for cool-season tornado events in that 10-yr period (18 in the WA region and 14 in the SA region). This sample comprised 11 F0, 12 F1, 7 F2, and 2 F3 tornadoes. Upper-air temperature data were available 12 hourly (at some stations) or 24 hourly, and vertical wind profiles were available at 6-h intervals. The nearest (in time and space) thermodynamic and wind sounding to the tornado location was modified to reflect surface conditions in the area

prior to the tornado. The mean buoyancy and shear values for various layers based on this set of modified proximity soundings are summarized in Table 1, while scatterplots of CAPE versus 0–1-km positive shear are shown in Fig. 13a (WA cases) and Fig. 13b (SA cases). The CAPE was calculated on the basis of a surface lifted parcel, using the virtual correction. Three of the F0 tornadoes in the WA dataset occurred with cyclonically turning wind profiles (cold advection) and were not included in the positive shear averages.

There are two clear differences between the SA and the WA cases. First, only 1 of the 14 SA tornadoes is rated F0, while 7 of the 15 WA tornadoes are rated F0. It is difficult to be certain whether this is due to random differences in the samples, to issues related to the reporting of events, or to differences in the climatologies of severe convection in the two regions. Bias in the reporting is most likely [comparable local biases occur within the U.S. tornado dataset, as discussed by Grazulis (1993, p. 93 ff.)], but the other factors cannot be ruled out. Second, there is a clear difference between the mean shears for the WA and the SA events, with the SA events showing a lower mean shear. Again, this may be due to sampling errors or may indicate a difference in the climatology of the two regions.

Events were associated with relatively low values of CAPE. SLI values were near neutral to slightly positive at 500 hPa, but were slightly negative at 700 hPa, indicating the bulk of the buoyancy for these events was concentrated in the lower levels (cf. Figs. 6 and 9). The greatest shear values were found in the 0–1-km layer. In the WA cases, 0–1-km shears were also stronger for the F1–F3 cases than for the F0 cases. Figure 13 shows that, while there is little association between F rating and CAPE, there does appear to be a tendency for the more destructive tornadoes to be associated with higher values of 0–1-km shear. Further, all events occurred with a 0–1-km shear greater than about $1.0\text{--}1.5 \times 10^{-2} \text{ s}^{-1}$. Box and whiskers plots for the WA events grouped according to F rating (Fig. 14) confirm the largest shear values are in the 0–1-km layer and indicate that the more destructive tornadoes ($>F0$) are associated with stronger 0–1-km (and 0–2 km) shears.

c. 30-yr analysis of annual number of days when shear and buoyancy criteria are met

The negative 700-hPa SLI/ shear $> 10^{-2} \text{ s}^{-1}$ conditions identified in the preceding section represent only

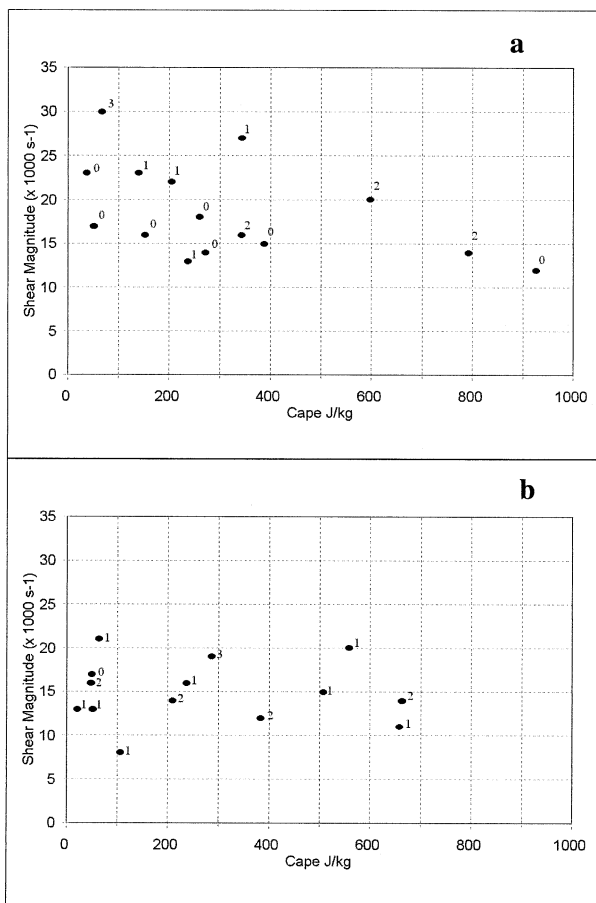


FIG. 13. Plot of 0–1-km positive shear vs CAPE for (a) WA and (b) SA tornado events. Numbers indicate Fujita intensity estimates. Shear units: 10^{-3} s^{-1} .

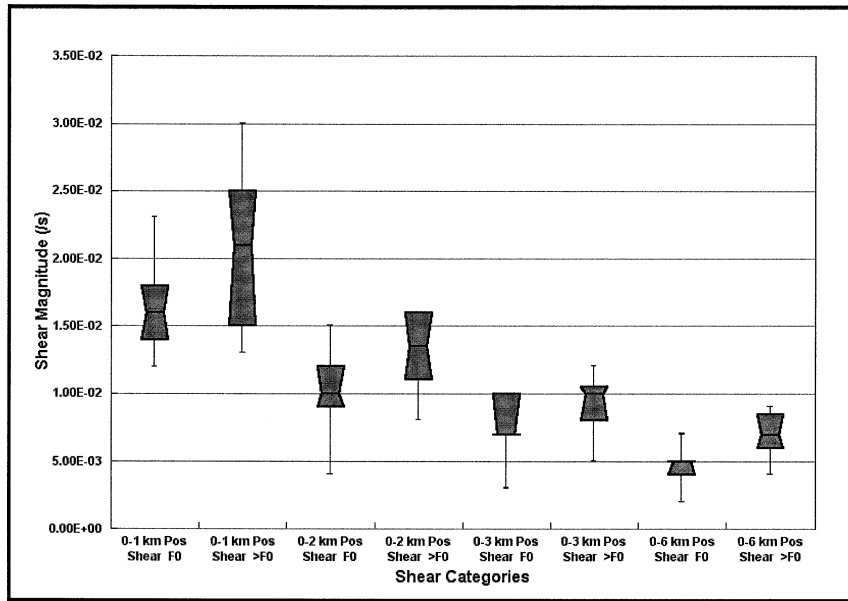


FIG. 14. Maximum, 75th, and 25th percentile and minimum values of positive shear for various layers for both weak and strong WA tornadoes.

observed tornadic thunderstorms. If these criteria are to be useful in identifying and forecasting potential tornadic thunderstorm environments, then it must be demonstrated that the results of the proximity sounding analysis did not occur by chance. The climatology of the number of days during May to September when 0–1-km shear $> 15 \text{ m s}^{-1}$ occurred in conjunction with 700-

hPa SLI < 0 provides some measure of this. Data used were 6-h radar wind observations and 12-h rawinsonde temperature soundings for the period 1967–97. No data were available for 1992. Figure 15 shows that the highest frequencies occur south of Adelaide and south of Perth, with maxima around 8 days $(\text{yr})^{-1}$ in each of these regions; these numbers are on the same order as the numbers of observed events in Fig. 1. There is also a close match between this spatial distribution and the distribution of *observed* events in Fig. 2. The monthly frequency of potential tornado days peaks in July at Perth and Albany, and in July–August at Adelaide and Mount Gambier. Note a small secondary maximum in Fig. 15 on the east coast of Australia, near 30°S. This feature will be discussed later.

While this analysis does not show that a high-shear environment necessarily leads to tornadic thunderstorms, it does indicate that a forecast tool based on these buoyancy/shear criteria could predict the climatological spatial and temporal distribution of cool-season tornadoes in Australian reasonably well.

4. Application to NWP forecasts

The Australian case studies presented above, and the observed values of SLI and low-level shear (see Table 1), occur in environments that might reasonably be expected to be resolved by current operational regional and mesoscale NWP models. First, assimilated analyses for the two cases described in sections 2b,c will be presented. A composite and a shear/buoyancy description of the NWP analyses for 21 Australian events will follow, and these results will be applied in daily forecasts for the winter of 1996.

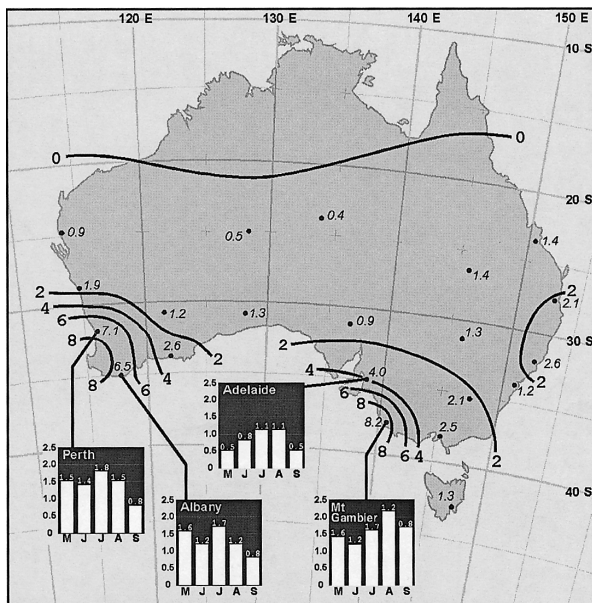


FIG. 15. Annual average number of cool-season days with 0–1.5-km shear $> 15 \text{ m s}^{-1}$ and 700-hPa SLI < 0 for southern Australian upper-air stations in the period 1967–97. The numbers mark the locations of Australian rawinsonde stations south of 20°S. Contours are in units of days per season.

Since July 1996, the operational regional NWP system used in Australia has been the BoM Limited Area Prediction System (LAPS), described in detail by Puri et al. (1998). At the time of this study, it had a horizontal grid spacing of 0.75° , and 19 vertical sigma levels. The initialization phase comprises three 6-h cycles of intermittent data assimilation (see Fig. 6 of Puri et al. 1998), commencing 12 h prior to the forecast base time ($t = 0$). The BoM global NWP model (Bourke et al. 1995) provides the background field for the initial analysis and the lateral boundary conditions for the subsequent 48-h forecast. As argued by, for example, Mills (1997), the advantage of using assimilated analyses in diagnostic studies is that the analyses use all available data, and so accurately reflect the observations, but also have a strong dynamic consistency enforced by the use of the numerical model used to link the analyses. The analyses used in these studies were either from the second or third assimilation cycle, depending on which was closest to the observed time of the tornado occurrence. In each case, then, the assimilation had at least one analysis-forecast cycle to achieve dynamic balance.

Of the 32 cases used in the observational analysis in Section 3b, there were 21 cases from the winters of 1994–96 (inclusive) for which LAPS assimilated analyses were either archived or could be rerun in an operationally identical mode. Prior to that time, changes in regional NWP systems made rerunning extremely complex, and use of earlier archived regional NWP analyses would have introduced marked inhomogeneity into this 21-case development dataset that is used in the following analysis.

The objective analyses for the WA and SA tornadic thunderstorm events described in sections 2b,c both show a very deep low pressure system to the south of the reported tornado location (Figs. 16a, 17a) and wind speeds at 950 hPa above 20 m s^{-1} (Figs. 16b, 17b). In each case, the tornadic storms occurred near the axis of a band of very strong 10-m–850-hPa shear ($>15 \text{ m s}^{-1}$; Figs. 16e, 17e), and on the cyclonic shear side of a very strong ($>70 \text{ m s}^{-1}$) northwesterly jet streak (Figs. 16d, 17d). In the WA case, the 700-hPa SLI (calculated from the lowest model level, around 70 m) is negative (Fig. 16c), but the SA case shows positive LI at the location of the tornadoes at 0500 UTC (Fig. 17c). However, the SA tornadoes were reported some 2 h after the analysis time, and the pattern of 700 LI suggests that destabilization likely occurred. These features are all consistent with the observationally based diagnoses in section 2.

The objective analyses also show low-level convergence (Figs. 16b, 17b) and upper-level divergence (Figs. 16d, 17d) on the cyclonic flank of the upper jet streak. The low-level convergence and upper-level divergence patterns suggest a coupling between the upper- and lower-tropospheric jet streaks, with a deep-tropospheric vertical circulation likely in the region where the storms occurred.

Subjectively, there was a surprising degree of simi-

larity in the synoptic patterns for each of the 21 cases. To test the rigor of this impression, the objective analysis fields for each of the 21 Australian cases were composited relative to the tornado location, or the centroid if there were more than one reported tornado for a given event. Fields were composited on the same 0.75° grid spacing as the LAPS model, and over a 37×37 (27° latitude–longitude) grid array. Some small error is introduced in the averaging because of the latitudinal variation of east–west grid spacing, but because most events were clustered fairly closely over southwestern WA or central SA, it is felt that this could be accepted for the qualitative analysis here. Fields composited were mean sea level pressure (MSLP), geopotential height, zonal and meridional wind components, temperature, and mixing ratio. Compositing was done only after each analysis was interpolated from model sigma coordinates to pressure levels, to avoid issues of varying topographic height.

Allowing for the care with which composites must be treated, and given the relatively small size of the samples, remarkably similar patterns for the WA (Fig. 18) and SA composites (Fig. 19) were found, confirming the subjective impressions gained from assessing individual cases. In addition the composites bear a striking similarity to the California conceptual model of LM. The composite analyses show that the events occurred

- around 10° latitude equatorward of an intense mid-latitude cyclone (Figs. 18a, 19a),
- immediately downstream of a very strong low-level isotach maximum (Figs. 18b, 19b),
- close to the axis of the strongest surface-to-850-hPa wind shear (Figs. 18e, 19e),
- with negative 700-hPa SLI just upstream (Figs. 18d, 19d),
- with a low-level convergence maximum over the event location (Figs. 18b, 19b),
- downstream of a sharply diffluent upper trough (Figs. 18c, 19c),
- below the cyclonic shear side of a strong jet streak (Figs. 18c, 19c), and
- on the axis of a low-level equivalent potential temperature (θ_e) maximum (Figs. 18f, 19f).

Ageostrophic analysis (not shown) indicates a coupling of the upper and lower jet streaks via a vertical circulation that not only assists the low-level convergence, but also assists the maintenance of the low-level wind shear. In both composites (Figs. 18f, 19f) a positive low-level (950 hPa) θ_e anomaly is seen across the tornado location. Although this feature was not identified in the case studies presented in sections 2b,c and in Figs. 16 and 17, these surface anomalies must contribute to the buoyancy seen in the proximity sounding data (Fig. 13).

Because the aim of this analysis is to derive a *forecast* product, the 700-hPa SLI and 10-m–850-hPa shear values were extracted from the objective analyses at the tornado locations, following the results of the prox-

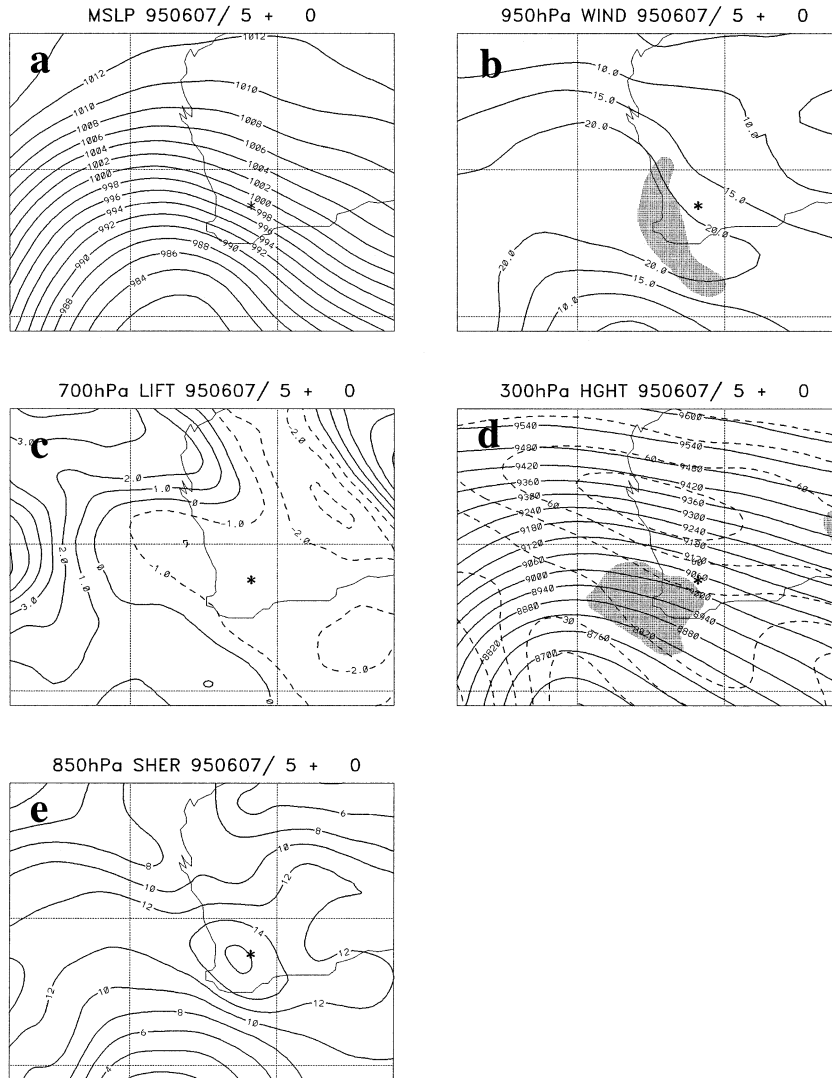


FIG. 16. LAPS analysis fields for 0500 UTC 7 Jun 1995. The asterisk marks the reported location of the tornado: (a) mean sea level pressure, contour interval 2 hPa; (b) 950-hPa wind speed (m s^{-1}), contour interval 5 m s^{-1} , with shaded areas showing 950-hPa divergence less than $-20 \times 10^{-6} \text{ s}^{-1}$; (c) 700-hPa SLI ($^{\circ}\text{C}$), negative contours dashed; (d) 300-hPa height (solid contours, interval 60 m), isotachs (dashed contours, interval 10 m s^{-1}), and shaded areas of divergence greater than $20 \times 10^{-6} \text{ s}^{-1}$; and (e) magnitude of 10-m–850-hPa wind shear (m s^{-1}), contour interval 2 m s^{-1} .

imity sounding analysis earlier. (It is not necessarily appropriate to use the values based on proximity soundings, for although the NWP analyses obviate the need for translation in space, the multivariate analysis and the scaling assumptions used in the analysis may reduce the fit of the analyses to the observations.) In addition, taking advantage of the internal dynamic consistency of the assimilated analyses, a convergence criterion—another necessary ingredient for convection—is included. It was found that a parameter space that encompassed

$700\text{-hPa SLI} < 0.0,$
 $950\text{-hPa divergence} < -5.0 \times 10^{-3} \text{ s}^{-1},$ and
 $\text{surface-to-850-hPa shear} > 8.0 \text{ m s}^{-1}$
 captured 19 of the 21 events in the development dataset (a “weak” signal), and
 $700\text{-hPa SLI} < -1.0,$
 $950\text{-hPa divergence} < -15.0 \times 10^{-3} \text{ s}^{-1},$ and
 $\text{surface-to-850-hPa shear} > 11.0 \text{ m s}^{-1}$

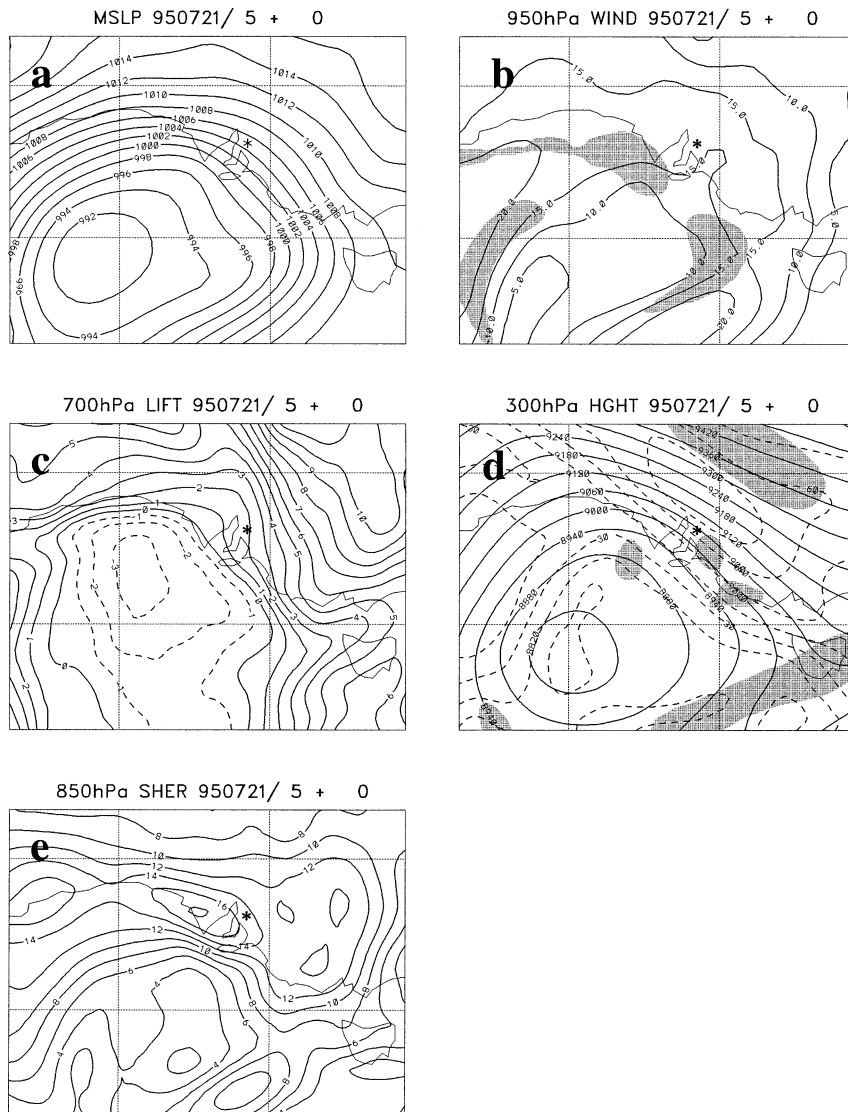


FIG. 17. LAPS analysis fields for 0500 UTC 21 Jul 1995. The asterisk marks the reported location of the tornado: (a) mean sea level pressure, contour interval 2 hPa; (b) 950-hPa wind speed (m s^{-1}), contour interval 5 m s^{-1} , with shaded areas showing 950-hPa divergence less than $-20 \times 10^{-6} \text{ s}^{-1}$; (c) 700-hPa SLI ($^{\circ}\text{C}$), negative contours dashed; (d) 300-hPa height (solid contours, interval 60 m), isotachs (dashed contours, interval 10 m s^{-1}), and shaded areas of divergence greater than $20 \times 10^{-6} \text{ s}^{-1}$; and (e) magnitude of 10-m–850-hPa wind shear (m s^{-1}), contour interval 2 m s^{-1} .

described a “strong” signal, and captured 9 of the 21 events. While the precise values of these thresholds are somewhat arbitrary, the first set of values is designed to maximize the probability of detection in the development data while maintaining the physical basis implied by the observational studies. The second set of thresholds is designed to match the proximity sounding values and reduce the size of the areas forecast, potentially reducing the false-alarm ratio at the expense of missing some events. It is acknowledged that there is scope for refinement in the choice of these values: however, apart from the convergence criteria, they agree

quite well with those determined from proximity data, as described in section 3.

To test the potential for the buoyancy/shear/convergence criteria identified from observations and objective analyses for known cases to *predict* cool-season tornado environments objectively, the parameters identified above were applied to the 24-h LAPS forecast based at 2300 UTC each day from 15 May to 15 September 1996 (123 forecasts). The 24-h period was chosen to provide adequate lead time to forecasters—regional NWP is not a nowcast tool—and the 2300 UTC time matches the observation time of the bulk of the Australian rawin-

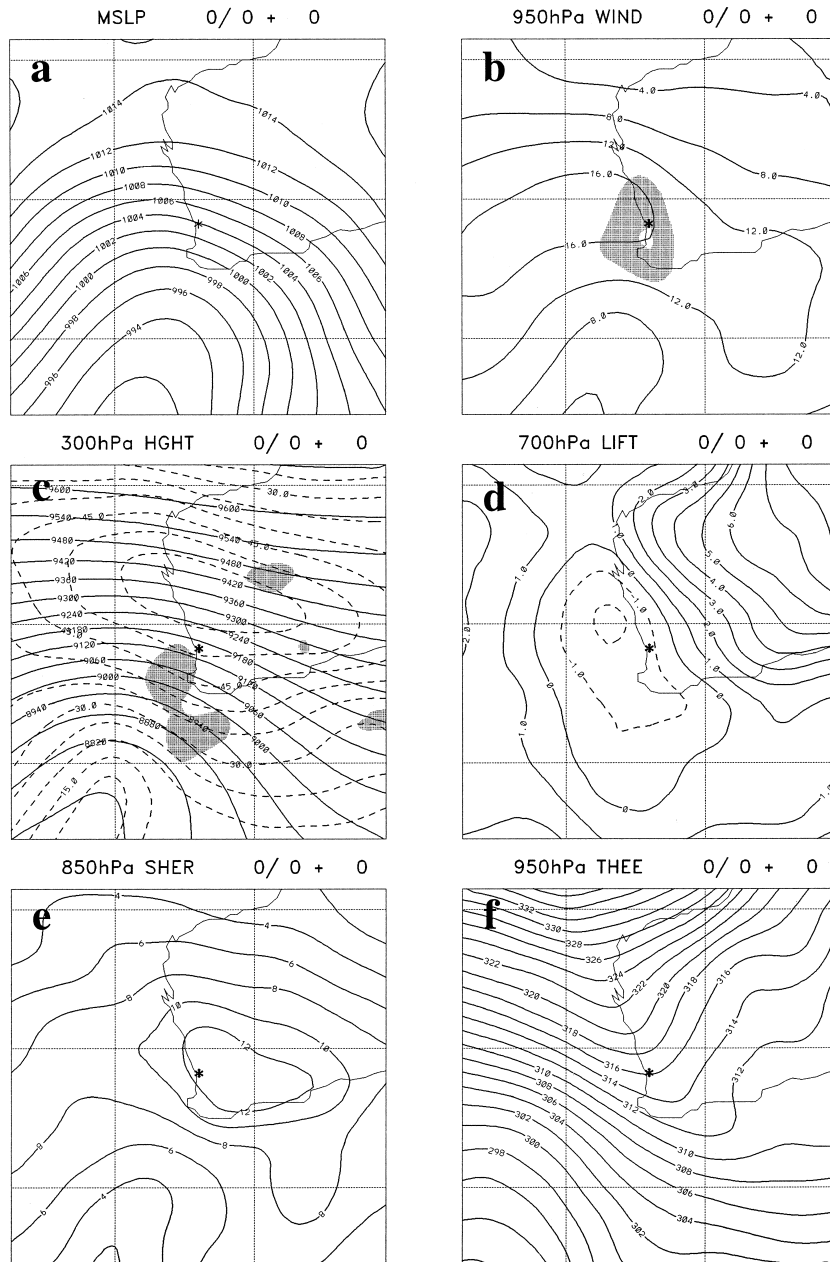


FIG. 18. Composite analysis fields for the WA cases. The asterisk marks the composite location, and has been placed at the location of Perth to provide a geographic reference: (a) mean sea level pressure, contour interval 2 hPa; (b) 950-hPa wind speed (m s^{-1}), contour interval 4 m s^{-1} , with shaded areas showing 950-hPa divergence less than $-10 \times 10^{-6} \text{ s}^{-1}$; (c) 300-hPa height (solid contours, interval 60 m), isotachs (dashed contours, interval 5 m s^{-1}), and shaded areas of divergence greater than $10 \times 10^{-6} \text{ s}^{-1}$; (d) 700-hPa SLI ($^{\circ}\text{C}$), negative contours dashed; (e) magnitude of 10-m–850-hPa wind shear (m s^{-1}), contour interval 2 m s^{-1} ; and (f) 950-hPa equivalent potential temperature, contour interval 2 K.

sonde network used in section 3c. Qualitative impressions are that this choice is not critical for this season-long assessment, because there is considerable temporal continuity of the spatial patterns of cool-season tornado potential in these NWP forecasts, although there are variations in detail in any individual case. In the test

period, there were nine tornado events reported in the BoM monthly significant weather summaries. For each of the nine individual forecasts valid near the time of these events, a “cool-season tornado environment” was forecast over the tornado event location: seven with a strong signal, and two with a weak signal. Six of these

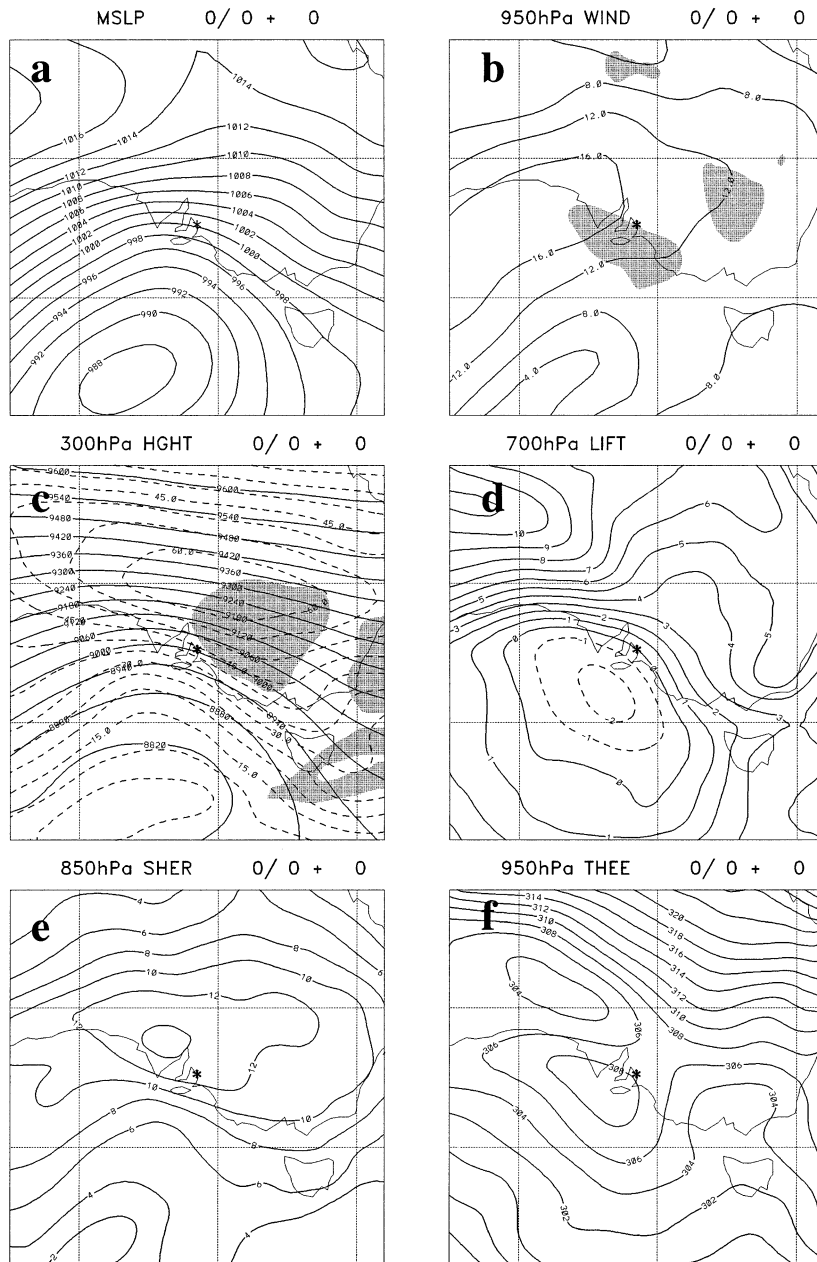


FIG. 19. Composite analysis fields for the SA cases. The asterisk marks the composite location and has been placed at the location of Adelaide to provide a geographic reference: (a) mean sea level pressure, contour interval 2 hPa; (b) 950-hPa wind speed (m s^{-1}), contour interval 4 m s^{-1} , with shaded areas showing 950-hPa divergence less than $-10 \times 10^{-6} \text{ s}^{-1}$; (c) 300-hPa height (solid contours, interval 60 m), isotachs (dashed contours, interval 5 m s^{-1}), and shaded areas of divergence greater than $10 \times 10^{-6} \text{ s}^{-1}$; (d) 700-hPa SLI ($^{\circ}\text{C}$), negative contours dashed; (e) magnitude of 10-m–850-hPa wind shear (m s^{-1}), contour interval 2 m s^{-1} and (f) 950-hPa equivalent potential temperature, contour interval 2 K.

events had also been included in the development sample; however, the development sample used the objective analyses, while these assessments are based on 24-h forecasts. This significantly reduces the dependency, as the data input to the forecasts were valid at least 24 h

prior to the time of the objective analysis used in developing the forecast criteria.

The results in the above paragraph indicate a very satisfactory probability of detection (POD) of a tornadic thunderstorm event. Unfortunately, it is much harder to

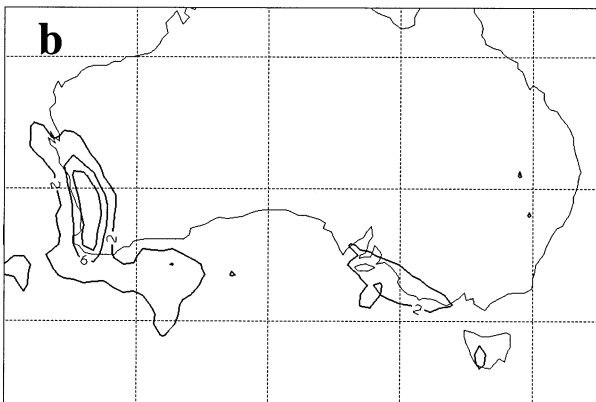
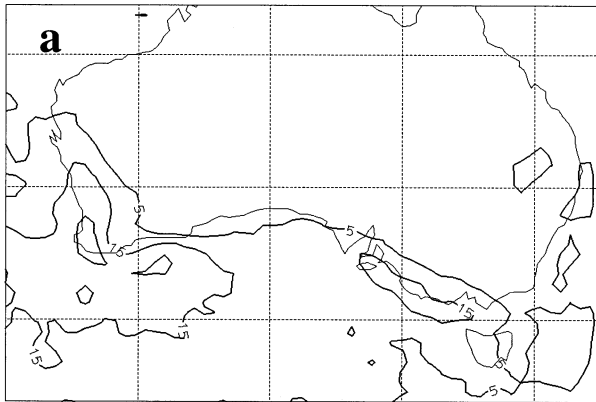


FIG. 20. Number of times during the period 15 May–15 Sep 1996 (123 forecasts) when a (a) strong or (b) weak forecast of cool-season tornado environment was made by a 24-h forecast based at 2300 UTC using LAPS. Contour intervals are (top) 10 and (bottom) 2. Lat–lon lines are at 10° intervals.

determine whether this excellent POD was achieved at the expense of an excessive false-alarm rate (FAR). This is because it is areas where there is *potential* for tornadic thunderstorms to occur (i.e., areas where shear, buoyancy, and convergence criteria are jointly satisfied) that are being forecast, rather than tornadic thunderstorms themselves. Accordingly, three further assessments were made.

First, the geographical distribution of the numerical predictions of cool-season tornado potential is assessed. The number of forecast hits at each grid point was summed for the 123 forecasts (Fig. 20). In Fig. 20a, either a weak or a strong forecast at a grid point was counted as a hit, whereas in Fig. 20b only the strong signals were counted as hits. In both cases, there is a remarkably similar pattern to that shown in Fig. 15, with maxima over southwest WA and over coastal south-eastern SA. Indeed, the number of “strong” signals is also similar in magnitude to the 30-yr observational

PERTH			ADELAIDE		
	FCST NO	FCST YES		FCST NO	FCST YES
OBS NO	99	11	OBS NO	113	1
OBS YES	3	10	OBS YES	3	5

ALBANY			MT. GAMBIER		
	FCST NO	FCST YES		FCST NO	FCST YES
OBS NO	115	7	OBS NO	114	6
OBS YES	1	0	OBS YES	2	1

FIG. 21. Contingency tables for the forecast of events at Perth, Adelaide, Albany, and Mount Gambier for which rawinsonde observations or numerical forecasts indicated that shear and buoyancy criteria were jointly satisfied.

climatology. This analysis supports the hypothesis that the LAPS predictions do not significantly overforecast using the criteria identified above. Figures 15 and 20 support the hypothesis that the patterns of tornado reports (Fig. 2) are *not* greatly skewed by the distribution of population in WA and SA. Further, it suggests that the differential friction across the ocean–land interface, and perhaps the northwest–southeast orientation of these coastlines, could play a role by enhancing the shear and ascent in those areas.

An interesting feature of this analysis is a small number of events that are forecast along the east coast of Australia, and just inland. This pattern is also seen in the 30-yr climatology in Fig. 15. These 1996 cases were associated with the strong winds in the southeast through southwest quadrants of low pressure systems in the easterly flow equatorward of the subtropical ridge.

Second, the number of days at the rawinsonde stations of Perth, Albany, Adelaide, and Mount Gambier (see Fig. 15 for locations) for which the model forecasts a strong signal at the rawinsonde location, or a weak signal at the rawinsonde location with an immediately adjacent strong signal, is verified against the number of days the rawinsonde data at those locations exceeded both shear and buoyancy thresholds. These data are shown in the contingency tables in Fig. 21. Several points can be made:

- As would be expected by a rare event forecast (Doswell et al. 1990), these tables are dominated by the no/no category at all four locations.
- There is some broad agreement between the station-to-station variations in the number of observed events and the number of predicted events, with Perth clearly being the largest in each category.
- For all stations, the POD is 0.64, while the FAR is 0.58. The resulting “skill”—as measured by the critical success index (CSI)—is 0.32, where 1.0 indicates

perfect forecasts and 0.0 is no better than random guessing.

There is no forecast product in the United States suite of Storm Prediction Center (SPC) severe weather forecasts (see Ostby 1992) comparable to this diagnostic. The “outlook” forecasts are not just for tornadoes, but include all other forms of severe thunderstorm weather events. There are separate tornado watches, of course, but these are not issued routinely, rather only as they are perceived to be necessary. The locally issued National Weather Service (NWS) tornado warning is a very short timescale product, sent when tornadoes are already occurring or are imminent. Hence, it is not possible to compare POD and FAR values for this diagnostic directly to any operational product being issued by the NWS, either for the California tornadoes, or those anywhere in the United States. However, as a point of reference, tornado watches currently have a POD of about 0.4–0.5 (McCarthy et al. 1998), with a FAR of roughly 0.7 and CSI values of about 0.2. Thus, this diagnostic appears to be slightly more skillful than SPC tornado watches as a whole, but the small sample size makes it dubious to make detailed quantitative comparisons. That these results indicate accuracy for this diagnostic comparable to, or even better than, current SPC tornado watches must be considered encouraging.

Third, a subjective comparison was made between each forecast cool-season potential field and the infrared satellite imagery at the valid time of the forecast. A cool-season potential area was counted in a given forecast if there were three or more contiguous grid points with strong signals identified over land. If two separate areas were identified in individual forecasts, then these were counted separately. On 47 occasions, the criteria for a warning area were satisfied. In most cases the forecast environments were associated with an area of enhanced cumuliform activity in the cold air cumulus field associated with a major midlatitude trough. This could be at a time when the cloud feature was still a separate cluster of enhanced convection, when a “cold air comma cloud” had developed, or just after it had merged with a frontal cloud band in a process similar to an “instant occlusion.” This association should not be unexpected, as the composite results show that the cool-season tornadoes occurred beneath the cyclonic shear side of an upper-level jet streak. This is the typical location of such cloud signatures, which are known to be associated with cyclonic vorticity advection (CVA) maxima in the mid- to upper troposphere (Anderson and Veltishchev 1973; Young 1995).

These enhanced convective cloud patterns, and a forecast of cool-season tornado potential, could frequently be discerned up to 24 h before the tornado environment forecast was valid over land. This suggests that the satellite imagery might be able to provide independent evidence in support for the LAPS forecasts, which have been shown to resolve CVA maxima well over the

Southern Ocean (Mills 1997). Note that seven tornadoes were reported in the vicinity of Los Angeles in the case of comma cloud development described by Reed and Blier (1986).

The forecasts were assessed as *poor* if there was no clearly identifiable cloud feature associated with the forecast area, *fair* if there was a phase or an area difference, and *good* if the location and size of the cloud and the forecast areas were in good agreement. Of the 47 forecasts, 1 was rated poor, 19 fair, and 27 good. This third assessment shows an apparently large number of “yes” forecasts as a proportion of the total number of 24-h forecasts (47 out of 123). This is, in part, due to the relatively large geographic area surveyed (Fig. 20), and the relatively small size of the typical forecast area within that domain.

5. Comparison with other tornado environments

It has been demonstrated that California and southern Australian cool-season tornadoes occur in similar low-buoyancy/high-shear environments. In both these areas, the storms often occur with $CAPE < 500 \text{ J kg}^{-1}$. Interestingly, the observed shear thresholds are also similar, with 0–1-km shears greater than 10^{-2} s^{-1} . Lipari and Monteverdi (2000) show that the 0–1-km positive shears in California tornadic thunderstorm environments are at least as great as those of the Great Plains tornadic thunderstorm environment, although the Great Plains storms frequently have significantly greater buoyancy, particularly in spring and into the summer. JDL show that the CAPE values for their warm-season Great Plains tornadic thunderstorms are greater than 1000 J kg^{-1} . During the cool season, JDL’s dataset shows that a significant number of tornadic thunderstorms occurred with CAPE values less than 1000 J kg^{-1} , but these tend to have much higher values of 0–2-km wind shear than do their warm-season counterparts. Interestingly, the shear threshold below which no cool-season Great Plains tornadic thunderstorms are seen in JDL’s dataset is $1\text{--}1.2 \times 10^{-2}$ —a value very consistent with the results from the Australian and California studies. Indeed, both the California and Australian observational studies, and the results of the NWP prediction experiments, indicate that high values of 0–1-km positive shear have the potential to alert forecasters to the possibility of tornadic thunderstorms occurring in low-buoyancy environments.

The typical synoptic environment of the California tornadoes (see LM) is surprisingly similar to that shown in the composite analyses for the Australian cases (Figs. 18, 19), with an active trough–jet system close to the location of the event. In both areas, it appears that local influences act to enhance the low-level shear. In California, the enhancement is due to orographic effects (LM; Blier and Batten 1994), whereas in Australia, it appears that the land–sea interface, together with the orientation of the coastline, enhances the shear along the southwest WA and southeast SA coastlines. In ad-

dition, just east of Perth and just east of Adelaide are low, north–south-oriented, mountain ranges, typically around 300 m high, with abrupt escarpments to the coastal plains. It is quite conceivable that these escarpments also act to enhance the low-level shear in the typical northwesterly flows in which these storms occur. The highest concentration of observed Australian cool-season tornadoes is immediately west of these escarpments (Fig. 2), but these are also the areas of highest population density, and there is no obvious way to be certain that this is not just an artifact of the reporting bias associated with population centers.

Although the typical California and southern Australia synoptic patterns for these tornadic storms are very similar, both the observed 30-yr climatology of shear/SLI and the modeled winter 1996 climatology of shear/SLI/convergence show a secondary maximum near 30°S on the east coast of Australia. It is found that these environments are in the easterly (onshore) flow associated with east coast cyclones—a class of small, intense extratropical cyclones that have many similarities to the subtropical cyclones described by Ramage (1962). Tornadic thunderstorms in these situations have been reported by Zillman (1972), and another case associated with an intense east coast low occurred at Fingal Bay (near 32.5°S) on 30 June 1998. This synoptic pattern is totally different from that of the southern Australian cool-season extratropical cyclones that provided the basis for the shear and buoyancy criteria used in the trial forecasts. However, if the same physical ingredients are present, irrespective of how they were brought together by the synoptic pattern (see Doswell et al. 1996), then tornadic thunderstorms can result, and those ingredients can indicate the areas where these storms are likely both in observations (Fig. 15) and in NWP datasets (Fig. 20).

The low-buoyancy environment associated with tornadic events in northern and central California and in southern Australia during the cool season is similar in some respects to that observed by McCaul (1991) and McCaul and Weisman (1996) for tornadic supercells in low-buoyancy tropical cyclone environments. Although the landfalling tropical cyclone environment is very different from the midlatitude, cold-core trough pattern we have shown (cf. Figs. 18 and 19) and that shown in LM, the tropical cyclone environment has some similarity to that of the Australian east coast cyclones. In the strong onshore flow on the poleward side of these east coast cyclones, there are near-saturated relative humidities and near-constant θ_e with height (and thus low CAPE) as a consequence of the long fetch over relatively warm ocean prior to landfall. These environments also bear considerable similarity to the subtropical rainband cloud modeling studies of Trier and Parsons (1995), where intense thunderstorm updrafts were simulated in high-shear environments.

McCaul and Weisman (2001) show in their modeling studies that in low-CAPE simulations “a clear mode of intense but shallow supercellular convection” can occur

“when both the buoyancy and ambient vertical shear are concentrated in the lower troposphere.” These authors then draw allusions to this mode of supercellular convection and the landfalling tropical cyclone environment (see above), and to the California case of Mon-teverdi and Quadros (1994).

6. Conclusions

The climatology and case studies over Australia have added to the number of examples in the literature of tornadic thunderstorms occurring in low-buoyancy/high-shear environments, in contrast to the high-buoyancy/high-shear environment of the Great Plains spring and early summer supercell events. The studies in both California and Australia show that these cool-season storms occur with CAPE values typically 200–400 J kg⁻¹, slightly negative 700-hPa SLI, and with 0–1-km shear of greater than 10⁻² s⁻¹. It has been shown that buoyancy does not necessarily discriminate between more and less damaging storms, but that the 0–1-km positive shear does provide such discrimination. Clearly, forecasters need to be alert to the possibility of such storms occurring in these low-buoyancy environments.

Both the California and Australian cases show very similar synoptic patterns in which their cool-season tornadic thunderstorms occur, and it appears that topographic forcing plays a role in enhancing the low-level shear, thus leading to locally preferred areas for cool-season tornado occurrence. However, when the parameters listed above are applied to climatological or NWP datasets, another synoptic environment, that of the Australian east coast cyclone (which is similar to that tropical cyclones), is also shown to have the potential for low-buoyancy tornadic thunderstorms. Thus the use of NWP model forecast fields of the *ingredients* identified from observational studies, rather than the synoptic pattern, has the potential to identify a range of synoptic environments or geographic regions with enhanced probability of tornadic events. The potential to identify the unusual situation, as well as the one that fits a single synoptic conceptual model, is particularly attractive.

Twenty-four-hour regional NWP forecasts for the Australian winter of 1996 were used to predict areas where 700-hPa SLI, surface–850-hPa shear, and near-surface convergence criteria were all satisfied, and these areas are shown to provide useful forecast guidance for cool-season tornado environments. Following real-time trials based on the 0.25° resolution meso-LAPS model during the winters of 1998 and 1999, and positive forecaster response, this product became part of the operational forecast suite of the BoM before the 2000 winter. Evaluation and refinement of these products and threshold criteria used will continue.

Acknowledgments. The Australian part of this work was initiated when Barry Hanstrum was attached to BMRC in Melbourne for a 3-month period during 1997.

The visit was undertaken through the cooperation of the Perth Regional Office, BMRC, and Services Policy Branch of the BoM. Mr. Kevin Smith from the Perth Severe Weather Section provided expert technical support. The authors acknowledge the thoroughness of the anonymous referees, whose suggestions have greatly improved the presentation of this paper.

REFERENCES

- Anderson, R. K., and N. F. Veltishchev, Eds., 1973: *The Use of Satellite Pictures in Weather Analysis and Forecasting*. World Meteorological Organization Tech. Note 124, 275 pp.
- Blier, W., and K. A. Batten, 1994: On the incidence of tornadoes in California. *Wea. Forecasting*, **9**, 301–315.
- Bourke, W., T. Hart, P. Steinle, R. Seaman, G. Embery, M. Naughton, and L. Rikus, 1995: Evolution of the Bureau of Meteorology's global assimilation and prediction system. Part 2: Resolution enhancements and case studies. *Aust. Meteor. Mag.*, **44**, 19–40.
- Brook, R. R., 1965: Tornado at Mandurah, 15 June 1964. *Aust. Meteor. Mag.*, **13** (50), 26–34.
- Carbone, R. E., 1983: A severe frontal rainband. Part II: Tornado parent vortex circulation. *J. Atmos. Sci.*, **40**, 2639–2654.
- Clarke, R. H., 1962: Severe local wind storms in Australia. CSIRO Division of Meteorological Physics Tech. Paper 13, 56 pp. [Available from CSIRO Atmospheric Research, PMB 1, Aspendale, VIC 3195, Australia.]
- Davies-Jones, R. P., 1986: Tornado dynamics. *Thunderstorm Morphology and Dynamics*, E. Kessler, Ed., University of Oklahoma Press, 197–236.
- Doswell, C. A., III, R. Davies-Jones, and D. L. Keller, 1990: On summary measures of skill in rare event forecasting based on contingency tables. *Wea. Forecasting*, **5**, 576–585.
- , H. E. Brooks, and R. A. Maddox, 1996: Flash flood forecasting: An ingredients-based methodology. *Wea. Forecasting*, **11**, 560–581.
- Foley, G. R., and B. N. Hanstrum, 1990: Severe local wind storms over southwestern Australia during the cooler months. *Proc. Second Australian Severe Thunderstorm Workshop*, Melbourne, Victoria, Australia, Bureau of Meteorology, 42–68. [Available from Bureau of Meteorology, Box 1289K, Melbourne, VIC 3001, Australia.]
- Grazulis, T. P., 1993: *Significant Tornadoes, 1680–1991*. Environmental Films, 1326 pp.
- Hanstrum, B. N., 1994: The Mandurah tornado of 21 September 1994. *Proc. Fourth Australian Severe Thunderstorm Conf.*, Mount Macedon, Victoria, Australia, Bureau of Meteorology, 89–107. [Available from Bureau of Meteorology, Box 1289K, Melbourne, VIC 3001, Australia.]
- , G. A. Mills, and A. Watson, 1998: Australian cool season tornadoes. Part 1: Synoptic climatology. Preprints, *19th Conf. on Severe Local Storms*, Minneapolis, MN, Amer. Meteor. Soc., 97–100.
- Hart, J. A., and W. D. Korotky, 1991: The SHARP Workstation v1.50. A skew-*T*/hodograph analysis and research program for IBM and compatible PCs. User's manual. NOAA/NWS Forecast Office, Charleston, WV, 62 pp.
- Johns, R. H., and C. A. Doswell III, 1992: Severe local storms forecasting. *Wea. Forecasting*, **7**, 588–612.
- , J. M. Davies, and P. W. Leftwich, 1993: Some wind and instability parameters associated with strong and violent tornadoes. 2: Variations in the combinations of wind instability parameters. *The Tornado: Its Structure, Dynamics, Prediction, and Hazards, Geophys. Monogr.*, No. 79, Amer. Geophys. Union, 583–590.
- Lipari, G. S., and J. P. Monteverdi, 2000: Convective and shear parameters associated with northern and central California tornadoes during the period 1990–94. Preprints, *20th Conf. on Severe Local Storms*, Orlando, FL, Amer. Meteor. Soc., 518–521.
- McCarthy, D., J. Schaefer, and M. Kay, 1998: Watch verification at the Storm Prediction Center 1970–1997. Preprints, *19th Conf. on Severe Local Storms*, Minneapolis, MN, Amer. Meteor. Soc., 603–606.
- McCaul, E. W., Jr., 1991: Buoyancy and shear characteristics of hurricane-tornado environments. *Mon. Wea. Rev.*, **119**, 1954–1978.
- , 1993: Observations and simulations of hurricane-spawned tornadoes. *The Tornado: Its Structure, Dynamics, Prediction and Hazards, Geophys. Monogr.*, No. 79, Amer. Geophys. Union, 119–142.
- , and M. L. Weisman, 1996: Simulations of shallow supercell storms in landfalling hurricane environments. *Mon. Wea. Rev.*, **124**, 408–429.
- , and —, 2001: The sensitivity of simulated supercell structure and intensity to variations in the shapes of environmental buoyancy and shear profiles. *Mon. Wea. Rev.*, **129**, 664–687.
- Mills, G. A., 1997: Studies of cva maxima south of Australia. Part I: A long-lived enhanced cumulus signature and induced cyclogenesis. *Aust. Meteor. Mag.*, **46**, 87–107.
- Monteverdi, J. M., and J. Quadros, 1994: Convective and rotational parameters associated with three tornado episodes in northern and central California. *Wea. Forecasting*, **9**, 285–300.
- , and S. Johnson, 1996: A supercell with hook echo in the San Joaquin valley of California. *Wea. Forecasting*, **11**, 246–261.
- Ostby, F. P., 1992: Operations of the National Severe Storms Forecast Center. *Wea. Forecasting*, **7**, 546–563.
- Phillips, E. F., 1965: The Nurmurkah tornado of August 1964. *Aust. Meteor. Mag.*, **13** (48), 37–45.
- Puri, K., G. D. Dietachmeyer, G. A. Mills, N. E. Davidson, R. A. Bowen, and L. W. Logan, 1998: The new BMRC Limited Area Prediction System, LAPS. *Aust. Meteor. Mag.*, **47**, 203–223.
- Ramage, C. S., 1962: The subtropical cyclone. *J. Geophys. Res.*, **67**, 1401–1411.
- Reed, R. J., and W. Blier, 1986: A further study of comma cloud development in the eastern Pacific. *Mon. Wea. Rev.*, **114**, 1696–1708.
- Rotunno, R., and J. B. Klemp, 1982: The influence of shear-induced pressure gradient on thunderstorm motion. *Mon. Wea. Rev.*, **110**, 136–151.
- Trier, S. B., and D. B. Parsons, 1995: Updraft dynamics within a numerically simulated subtropical rainband. *Mon. Wea. Rev.*, **123**, 39–58.
- Watson, A., 1985: An examination of three winter tornadoes in southwest Western Australia. Meteorological Note 162, Bureau of Meteorology, 43pp. [Available from Bureau of Meteorology, Box 1289K, Melbourne, VIC 3001, Australia.]
- , 1996: The tornado outbreak of 21 July 1995—Boundary layer vorticity and storm relative helicity influences. *Proc. Fifth Australian Severe Thunderstorm Conf.*, Avoca Beach, New South Wales, Australia, Bureau of Meteorology, 53–57. [Available from Bureau of Meteorology, Box 1289K, Melbourne, VIC 3001, Australia.]
- Wicker, L. J., and L. Cantrell, 1996: The role of vertical buoyancy distributions in miniature supercells. Preprints, *18th Conf. on Severe Local Storms*, San Francisco, CA, Amer. Meteor. Soc., 225–229.
- Young, M. V., 1995: Depressions in mid-latitudes. *Images in Weather Forecasting*, M. J. Bader et al., Eds., Cambridge University Press, 206–286.
- Zillman, J. W., 1962: Report on tornado investigation—Port Macquarie, July 1962. *Aust. Meteor. Mag.*, **10** (39), 28–48.